Eupalinolide A induces autophagy via the ROS/ERK signaling pathway in hepatocellular carcinoma cells *in vitro* and *in vivo*

YONGHUI ZHANG[1-3], FENG DONG[1,2], ZHIHAO CAO[1,2], TINGTING WANG[1,2], LIAN PAN[1,2], WUJING LUO[1,2], WENXUAN DING[1,2], JIAXIN LI[1,2], LISHAN JIN[1,2], HUAN LIU[1,2], HAOYANG ZHANG[1,2], JINAGE MU[1,2], MEIYUE HAN[1,2], YONG WEI[4], XUESONG DENG[1,2], DAN LIU[1,2], PO HAO[1,2], GANG ZENG[1,2], YI PANG[1,2], GUIYUAN LIU[1,2,5] and CHANGLIN ZHEN[1,2]

[1]Chongqing Key Laboratory of Development and Utilization of Genuine Medicinal Materials in Three Gorges Reservoir Area; [2]Chongqing Engineering Research Center of Antitumor Natural Drugs, Chongqing Three Gorges Medical College, Chongqing 404120; [3]Hepatological Surgery Department, The First Affiliated Hospital of Chongqing Medical University, Chongqing 400042; [4]Key Laboratory of Intelligent Information Processing and Control, College of Electronic and Information Engineering, Chongqing Three Gorges University, Chongqing 404110; [5]General Surgery Department, The Affiliated Hospital of Chongqing Three Gorges Medical College, Chongqing 404000, P.R. China

Received May 20, 2022; Accepted August 17, 2022

DOI: 10.3892/ijo.2022.5421

Abstract. Hepatocellular carcinoma is the most common primary malignancy of the liver. The current systemic drugs used to treat hepatocellular carcinoma result in low overall survival time. It has therefore been suggested that new small-molecule drugs should be developed for treating hepatocellular carcinoma. *Eupatorium lindleyanum* DC. (EL) has been used to treat numerous diseases, particularly respiratory diseases; however, to the best of our knowledge, studies have not yet fully elucidated the effect of EL on hepatocellular carcinoma. In the present study, the effect of eupalinolide A (EA), one of the extracts of EL, was evaluated on tumor growth in a xenograft model of human hepatocellular carcinoma cells, and on the proliferation and migration of hepatocellular carcinoma cell lines. Cell cycle progression and the type of cell death were then evaluated using the Cell Counting Kit 8 assay, flow cytometry, electron microscopy and western blotting. EA significantly inhibited cell proliferation and migration by arresting the cell cycle at the G_1 phase and inducing autophagy in hepatocellular carcinoma cells. EA-induced autophagy was mediated by reactive oxygen species (ROS) and ERK signaling activation. Specific inhibitors of ROS, autophagy and ERK inhibited EA-induced cell death and migration. In conclusion, the present study revealed that EA may inhibit the proliferation and migration of hepatocellular carcinoma cells, highlighting its potential as a promising antitumor compound for treating hepatocellular carcinoma.

Correspondence to: Professor Guiyuan Liu, General Surgery Department, The Affiliated Hospital of Chongqing Three Gorges Medical College, 38 Guanmenshi Road, Gaosuntang, Chongqing 404000, P.R. China
E-mail: liugy19@lzu.edu.cn

Dr Changlin Zhen, Chongqing Key Laboratory of Development and Utilization of Genuine Medicinal Materials in Three Gorges Reservoir Area, Chongqing Three Gorges Medical College, 366 Tianxing Road, Wanzhou, Chongqing 404120, P.R. China
E-mail: changlinzhen@cqtgmc.edu.cn

Key words: eupalinolide A, hepatocellular carcinoma, reactive oxygen species, autophagy, ERK

Introduction

Hepatocellular carcinoma is the most common type of primary liver cancer. Liver cancer is the second most common cause of cancer-related death and the fifth most common type of cancer in China (1). Patients in the early and intermediate stages of the disease are treated with curative intent through surgery and local ablation; however, the disease develops rapidly and is associated with a high level of recurrence. The advanced disease stages of liver cancer are treated by systemic therapy (2,3). Multi-kinase inhibitors have been approved as first-line therapy drugs (4). Sorafenib, regorafenib and lenvatinib, which are multi-kinase inhibitors, have all been approved as first-line treatments for primary hepatocellular carcinoma (5); however, these drugs are limited by poor overall survival, low objective response rate, hepatotoxicity and high cost (6,7). Developing new small-molecule drugs is thus of great clinical significance in treating hepatocellular carcinoma.

Eupatorium lindleyanum DC. (EL), also called 'Yemazhui', is a traditional Chinese medicine that has been used to treat cough and chronic bronchitis in China for several thousands of years (8). Scientists have isolated >100 compounds from EL, including sesquiterpenes, diterpenoids, triterpenoids and volatile oils, and sesquiterpenes are one of the most abundant ingredients. The present study investigated the effect of the sesquiterpene lactone constituent eupalinolide A (EA) on hepatocellular carcinoma. The constituents of EL have several

pharmacological effects, including anti-bronchitis, antihypertensive, antiviral and anti-lung cancer activities (9-11). Scientists have hypothesized that EL may alter the cell metabolism to treat rat hyperlipidemia (12). Furthermore, it has been suggested that EL extracts can exert antipyretic effects by inhibiting myeloperoxidase activity in the liver (13). However, the effects of EL on hepatocellular carcinoma remain largely unknown.

The present study investigated the effect and mechanism of action of EA on hepatocellular carcinoma. The pharmacological activity of EA on tumor growth was detected *in vivo* in a xenograft model of human hepatocellular carcinoma cells, whereas cell proliferation was evaluated *in vitro* using hepatocarcinoma cell lines (MHCC97-L and HCCLM3). The effect of EA on the cell cycle was then investigated, as well as on the type of cell death, including apoptosis, necrosis and autophagy. Cell migration was evaluated using the wound-healing and Transwell assays. Inhibitors of cell death, reactive oxygen species (ROS) and MAPK signaling pathways were used to identify the related mechanisms. EA exerted an inhibitory effect on hepatocellular carcinoma, highlighting its potential as a novel small-molecule anticancer compound. The present study may improve the information available regarding the effect of EA on hepatocellular carcinoma, allowing for further investigation.

Materials and methods

Cell culture and treatment. Human hepatocellular carcinoma cells MHCC97-L and HCCLM3 (Shanghai Zhongqiao Xinzhou Biotechnology Co., Ltd.) were cultured in DMEM (Gibco; Thermo Fisher Scientific, Inc.), and incubated at 37˚C in an atmosphere containing 5% CO_2. Media were supplemented with 10% fetal bovine serum (FBS; Gibco; Thermo Fisher Scientific, Inc.). EA was purchased from Chengdu Must Bio-Technology Co., Ltd. and was dissolved in DMSO before being used to treat the hepatocellular carcinoma cell lines MHCC97-L and HCCLM3 at different concentrations (7, 14 and 28 μM) at 37˚C for 24, 48 or 72 h, according to the subsequent experiment. The following inhibitors were used to treat the MHCC97-L and HCCLM3 cell lines for 30 min prior to EA treatment at 37˚C: Z-VAD-FMK (20 μM; MedChemExpress LLC), necrostatin-1 (30 μM; MedChemExpress LLC), 3-methyladenine (3-MA; 2 mM; MedChemExpress LLC), N-acetylcysteine (NAC; 3 mM; MilliporeSigma) and PD98059 (20 μM; MedChemExpress LLC). DMSO was used to treat the control group. All experiments were performed independently and in triplicate.

Microscopic observation. Hepatocellular carcinoma cells ($4x10^3$ cells/well) were seeded into six-well cell culture plates and incubated for 48 h after EA (7, 14 and 28 μM) and DMSO treatment. The cells were observed under a light inverted microscope (Leica Microsystems GmbH). Cell numbers were analyzed using Image-Pro Plus 7.0 software (Media Cybernetics, Inc.). The proliferation rate was calculated as follows: 100x (mean number of cells in the experimental group/mean number of cells in control group).

Cell Counting Kit 8 (CCK8) assay. The CCK8 (Dojindo Laboratories, Inc.) was used to determine the viability of MHCC97-L and HCCLM3 cells. Cells were seeded into 96-well culture plates at a density of 5,000 cells/well. EA was then added to the drug administration group at a final concentration of 7, 14 and 28 μM, and the cells were incubated for 24, 48 and 72 h at 37˚C. CCK8 solution (10 μl) was then added to each well and the cells were further incubated at 37˚ for 4 h. The OD value of the cells was measured at 450 nm using a microplate reader.

5-bromo-2-deoxyuridine (BrdU) staining. Cell proliferation was measured by BrdU staining. A total of $1x10^4$ cells were seeded in 24-well plates, followed by the addition of DMEM containing DMSO or EA (28 μM), and were incubated at 37˚C for 2 days. Subsequently, the cells were incubated with 10 μg/ml BrdU (MilliporeSigma) for 2 h at 37˚C and fixed with 4% paraformaldehyde for 15 min at room temperature. The cells were then treated with 2 M HCl at 37˚C for 30 min and blocked with 10% goat serum (OriGene Technologies, Inc.) containing 0.3% Triton X-100 for 1 h at room temperature. The cells were then incubated with BrdU primary antibody (1:1,000; cat. no. ab6326; Abcam) at 4˚C overnight and with an Alexa Fluor™ 594-conjugated goat anti-rat IgG secondary antibody (1:1,000; cat. no. A-11007; Thermo Fisher Scientific, Inc.) for 2 h at room temperature. The cells were finally stained with DAPI for 15 min at room temperature and observed under a fluorescence microscope. BrdU-positive cells in three random fields were counted. The cells were counted using Photoshop CC 2018 software (Adobe Systems, Inc.).

Soft agar assay. The effect of EA on the colony-forming ability of hepatocellular carcinoma cells was determined using the soft agar assay. Briefly, 1.5 ml 2X RPMI-1640 (Gibco; Thermo Fisher Scientific, Inc.) containing 0.6% agarose (MilliporeSigma) was added to 6-well plates as base agar at 37˚C for 1 h. A total of 10^3 cells and 28 μM EA were then added to the top of the base agar and incubated at 37˚C for 21 days. The hepatocellular carcinoma cells were finally stained with MTT for 30 min at 37˚C and were images were captured using a digital camera.

Wound-healing assay. Hepatocellular carcinoma cells were seeded in a 6-well plate and incubated until they reached 90% confluence. The cells were then scratched using a 100-μl sterile pipette tip to form a linear wound, followed by the addition of serum-free DMEM containing 7, 14 or 28 μM EA or DMSO. Cell migration across the wounded area was observed at 6, 24 and 48 h and the extent of wound closure was measured at the indicated time points (14). The cells were observed under a light inverted microscope (Leica Microsystems GmbH). Cell migration was analyzed using Image-Pro Plus 7.0 software. The wound closure rate was calculated as follows: Wound closure (%)=100x [scratch width at 0 h-scratch width at 6, 24 or 48 h)/(scratch width at 0 h)].

Cell migration. The migratory potential of hepatocellular carcinoma cells was measured using Transwell chambers (pore size, 8 μm; Corning, Inc.). Briefly, the hepatocellular carcinoma cells ($2x10^5$) were suspended in DMEM containing 1% FBS and were seeded into the upper chamber. DMEM (500 μl) containing 20% FBS was then added to the lower

chamber to act as a chemoattractant. The cells were incubated for 48 h with DMEM at 37˚C containing 7, 14 or 28 μM EA, or DMSO. Cells on the lower surface of the membrane were stained with 0.5% crystal violet for 15 min at room temperature. The cells were observed under an light inverted microscope (Leica Microsystems GmbH). Images of the stained cells were randomly captured and the cells were counted using the Image-Pro Plus 7.0 software. The migration rate was calculated as follows: 100x (mean number of migrating cells in the experimental group/mean number of migrating cells in control group).

Western blot analysis. Western blotting was performed as previously described (15). The cells were treated with EA (7, 14 and 28 μM) for 24 h. The treated cells were harvested and lysed on ice using RIPA lysis buffer (Beyotime Institute of Biotechnology) containing protease and phosphatase inhibitors (Roche Diagnostics). The protein concentration of the cell lysate was measured using the BCA protein assay kit (Beyotime Institute of Biotechnology). The cell lysate was then denatured at 100˚C for 5 min. Subsequently, 50 μg protein extracts were subjected to SDS-PAGE on 10 and 12% gels and were transferred onto a polyvinylidene difluoride membrane. The membrane was blocked in 5% bovine serum albumin (MilliporeSigma) at room temperature for 1 h, and was then incubated overnight at 4˚C with the following primary antibodies: E-cadherin (1:1,000; cat. no. 14472), Vimentin (1:1,000; cat. no. 5741T), cleaved-PARP (1:1,000; cat. no. 5625T), cleaved-caspase-3 (1:1,000; cat. no. 9661), autophagy-related 5 (Atg5; 1:1,000; cat. no. 12994T), p62 (1:1,000; cat. no. 8025T), MAPK family sampler kit (1:1,000; cat. no. 9926T), p-ERK (1:1,000; cat. no. 4370T), p-JNK (1:1,000; cat. no. 4668T), p-p38 (1:1,000; cat. no. 4511T), LC3B (1:1,000; cat. no. 12741), Cyclin D1 (1:1,000; cat. no. 55506), fibronectin (1:1,000; cat. no. 26836), CDK4 (1:1,000; cat. no. 12790), PARP (1:1,000; cat. no. 9542), caspase-3 (1:1,000; cat. no. 9662) (all Cell Signaling Technology, Inc.), CDK2 (1:500; cat. no. sc-6248), Cyclin E1 (1:500; cat. no. sc-247) (both Santa Cruz Biotechnology, Inc.), RIP1 (1:1,000; cat. no. CY6582), p-MLKL (1:1,000; cat. no. CY7146), MLKL (1:1,000; cat. no. CY5493) (all Shanghai Abways Biotechnology Co., Ltd.), N-cadherin (1:1,000; cat. no. AP71171), ZEB1 (1:1,000; cat. no. AM1878A) (both from Abcepta Biotech Ltd. Co.) and β-actin (1:1,000; cat. no. TA-09; OriGene Technologies, Inc.). The membrane was subsequently incubated with horseradish peroxidase-conjugated secondary antibodies [goat anti-mouse IgG (cat. no. A0216) and goat anti-rabbit IgG (cat. no. A0208); 1:10,000; Beyotime Institute of Biotechnology] at room temperature for 1 h. The protein bands were finally visualized using the Clarity Western ECL Blotting Substrate (cat. no. 1705061; Bio-Rad Laboratories, Inc.) and images were captured using a ChemiDoc MP Imaging System (Bio-Rad Laboratories, Inc.). The integrated optical density of the protein bands was measured using the Bio-Rad Image Lab Software 5.2.1 (Bio-Rad Laboratories, Inc.), with β-actin employed as the loading control.

Cell cycle analysis. Hepatocellular carcinoma cells were incubated for 48 h after EA (14 and 28 μM) at 37˚C and DMSO treatment. The treated cells at 70-80% confluence were fixed with 75% ethanol at 4˚C and then incubated in 500 μl PBS containing PI and RNase A (9:1) at 37˚C for 60 min (Cell Cycle Kit; Nanjing KeyGen BioTech Co., Ltd.). The cell samples were analyzed using DxFLEX flow cytometry (Beckman Coulter, Inc.). The cell percentage in each cycle was finally evaluated using Modfit-LT V 3.0 software (Verity Software House).

Analysis of cell apoptosis. Hepatocellular carcinoma cells were cultured for 48 h after EA (7, 14 and 28 μM) and DMSO treatment. The cells were then collected, washed with cold PBS and suspended in 200 μl binding buffer (Annexin V-FITC/PI apoptosis assay kit; Neobioscience Technology Co., Ltd.) at a density of $5x10^5$/ml. Subsequently, cells in binding buffer (195 μl) were incubated with 5 μl Annexin V-FITC at room temperature in the dark for 10 min. The cells were then washed with PBS, suspended in binding buffer, and mixed with 10 μl PI. The mixture was gently mixed and analyzed by DxFLEX flow cytometry. The apoptotic rate of the hepatocellular carcinoma cells was finally determined using CytExpert 2.0 software (Beckman Coulter, Inc.).

Transmission electron microscopy. Hepatocellular carcinoma cells were incubated for 48 h after EA (28 μM) and DMSO treatment. The cells at a density of 10^6/ml were then collected into a 1.5 ml Eppendorf tube containing trypsin and centrifuged at 100 x g for 5 min at room temperature. The supernatant was collected, and the cells were fixed with 1 ml 2.5% glutaraldehyde fixing solution for 1 h at 4˚C and treated with 1% OsO_4 in PBS for 1 h at 4˚C The cells were then dehydrated in ethanol, embedded in epoxy resin and sliced into 90-nm sections. The sections were stained with uranyl acetate for 5 min and lead citrate for 5 min at 37˚. Ultrathin sections of the cells were examined under a JEM1200EX transmission electron microscope (Jeol Ltd.).

ROS detection analysis. Hepatocellular carcinoma cells were incubated for 48 h after EA (14 and 28 μM) and DMSO treatment. The cells ($4x10^3$ cells/well) were seeded into six-well plates, then collected, suspended in serum-free DMEM containing 10 μM DCFH-DA (Reactive Oxygen Species Assay Kit; Beyotime Institute of Biotechnology) and incubated at 37˚C for 20 min. The cells were subsequently washed three times with serum-free cell medium and analyzed by DxFLEX flow cytometry. The ROS content in the hepatocellular carcinoma cells was finally analyzed using CytExpert 2.0 software.

RNA sequencing and data analysis. HCCLM3 cells were harvested after 48 h of treatment with DMSO and EA (14 and 28 μM) at 5% CO_2 and 37˚C for total RNA isolation using TRNzol Universal Total RNA extraction reagent (cat. no. DP424, Tiangen Biotech Co., Ltd.). RNA samples were submitted to Shanghai Personalbio Technology Co., Ltd. for transcriptome sequencing and analysis. The concentration, quality and integrity of RNA were determined using a NanoDrop spectrophotometer (Thermo Fisher Scientific, Inc.). Integrity was assessed by an Agilent 2100 Bioanalyzer using the RNA 6000 Nano kit (cat. no. 5067-1511) (both Agilent Technologies Inc.). Subsequently, 3 μg RNA was used as the input material for RNA sample preparation. The experiment was performed according to manufacturer's protocol of NEBNext Ultra II RNA Library Prep Kit for Illumina (cat.

no. E7775; New England Biolabs, Inc.). Sequencing libraries were generated according to the following steps. Firstly, mRNA was purified from total RNA using poly-T oligo-attached magnetic beads. Fragmentation was carried out using divalent cations under elevated temperature in an Illumina proprietary fragmentation buffer (Illumina, Inc.). First strand cDNA was synthesized using random oligonucleotides and Super Script II. Second strand cDNA synthesis was subsequently performed using DNA Polymerase I and RNase H. Remaining overhangs were converted into blunt ends via exonuclease/polymerase activities and the enzymes were removed. After adenylation of the 3' ends of the DNA fragments, Illumina PE adapter oligonucleotides (Illumina, Inc.) were ligated to prepare for hybridization. To select cDNA fragments of the preferred 400-500 bp in length, the library fragments were purified using the AMPure XP system (Beckman Coulter, Inc.).

DNA fragments with ligated adaptor molecules on both ends were selectively enriched using Illumina PCR Primer Cocktail (Illumina, Inc.) in a 15-cycle PCR reaction. Products were purified (AMPure XP system) and quantified using the Agilent High Sensitivity DNA assay on the 2100 Bioanalyzer system (both Agilent Technologies, Inc.). The sequencing library was then sequenced on the NovaSeq 6000 platform (Illumina, Inc.) by Shanghai Personal Technology Co. Ltd. To select cDNA fragments of the preferred 400-500 bp in length, the library fragments were purified using the AMPure XP system. The library was uniformly diluted to 2 nM and PE150 mode sequencing was performed on the Illumina sequencer.

The original off-machine data were filtered for the transcriptome analysis. The high-quality sequences obtained were aligned with the human reference genome (Homo_sapiens. GRCh38.dna.primary_assembly.fa). The expression levels of the genes were calculated based on the comparison results, followed by expression difference analysis between the EA (24 μM) and control group, enrichment analysis and cluster analysis between EA and Control groups. Gene read counts were estimated with HTSeq (0.9.1) statistics (16). FPKM was used to standardize the expression. The differential expression of genes was analyzed using DESeq 1.30.0 (Bioconductor) (16,17). The screening conditions were as follows: |log2FoldChange|>1 and significant P<0.05. The R language heatmap (1.0.8) software package was used to perform a bi-directional clustering analysis of all different genes in the samples (16). The heatmap was developed according to the expression levels of the same gene in different samples and the expression patterns of different genes in the same sample. The Euclidean method was used to calculate the distance and the complete linkage method was performed for clustering. ClusterProfiler (3.4.4) software was used to carry out the Kyoto Encyclopedia of Genes and Genomes (KEGG) pathway enrichment analysis of the differentially expressed genes, focusing on the pathways with P<0.05 (18-20).

Animal studies. A total of 36 female nude mice (BALB/c; weight 18-20 g; age, 4 weeks) were purchased from Cavensbiogle and housed in a specific pathogen-free room that was maintained at a constant temperature (20-26˚C) and humidity (40-70%). The mice were maintained under a 12-h light/dark cycle with free access to food and water. The animals were divided into three groups and the number of mice per group was six; the number of mice in the MHCC97-L group was 18 and the number of mice in the HCCLM3 group was also 18. MHCC97-L and HCCLM3 cells ($1x10^6$ cells in 200 μl PBS) were subcutaneously injected into the nude mice. The mice were then intraperitoneally injected with EA (30 or 60 mg/kg) and saline solution (Control) once per day for 3 weeks. The body weight of the mice was monitored, and the tumor size was measured to calculate the tumor volume, as follows: Volume=$4\pi/3$ x R^3, where R=L + W/2; R refers to the radius of tumor, L refers to the longest diameter of the tumor mass and W to the longest transverse diameter perpendicular to the longest diameter. Volume was calculated from day 12 to 26 (once every 2 days). The mice were euthanized using CO_2 (30% of the volume of the euthanasia chamber was replaced with CO_2 every minute) on day 26 (the maximum tumor volume of the MHCC97-L group was 810.41 mm^3 and the maximum tumor volume of the HCCLM3 group was 960.66 mm^3), and the tumors were subsequently excised and weighted.

Statistical analysis. Data were analyzed using GraphPad Prism 5.01 software (GraphPad Software, Inc.) and were presented as the mean ± SD. All experiments were repeated at least three times. Two groups were compared using an unpaired two-tailed Student's t-test. One-way ANOVA followed by Tukey's test was used to assess and compare the mean differences among multiple groups. P<0.05 was considered to indicate a statistically significant difference.

Results

EA inhibits the proliferation of human hepatocellular carcinoma cells in vitro. Hepatocellular carcinoma is characterized by rapid development and high mortality (21). Effective inhibition of tumor growth is therefore of great importance. The concentration of EA used in the present study was chosen based on relevant studies of EL extract and the IC_{50} of EA in MHCC97-L and HCCLM3 cells (Fig. S2B) (22,23). When the concentration of EA was ~10 μM, it could serve a significant inhibitory effect on hepatocellular carcinoma cell lines; therefore, the concentrations of EA used in the present study were selected. In the present study, MHCC97-L and HCCLM3 cells were treated with different concentrations of EA (7, 14 and 28 μM) for 48 h to investigate the anti-proliferative effects of EA on human hepatocellular carcinoma cells. DMSO was used as the control. The viability of hepatocellular carcinoma cells was examined through light morphological analysis, CCK8 assay, BrdU staining and soft agar assay. Microscopic examinations revealed that EA altered their morphology in a dose-dependent manner (Fig. 1A). Decreased cell number, cell shrinkage, dispersed cell growth and pleomorphic cell morphology were observed following EA treatment. Images of the cells were captured and the number of cells was statistically analyzed to obtain the proliferation rate. The proliferation rate was measured by comparing the proliferation of the DMSO group with that of the EA group and the proliferation rate was reduced following EA treatment (Fig. 1B). Notably, there was a significant decrease in the viability of the two cell lines treated with EA after 24, 48 and 72 h compared with that in the DMSO group (Fig. 1C). DNA synthesis in cells treated with EA was also

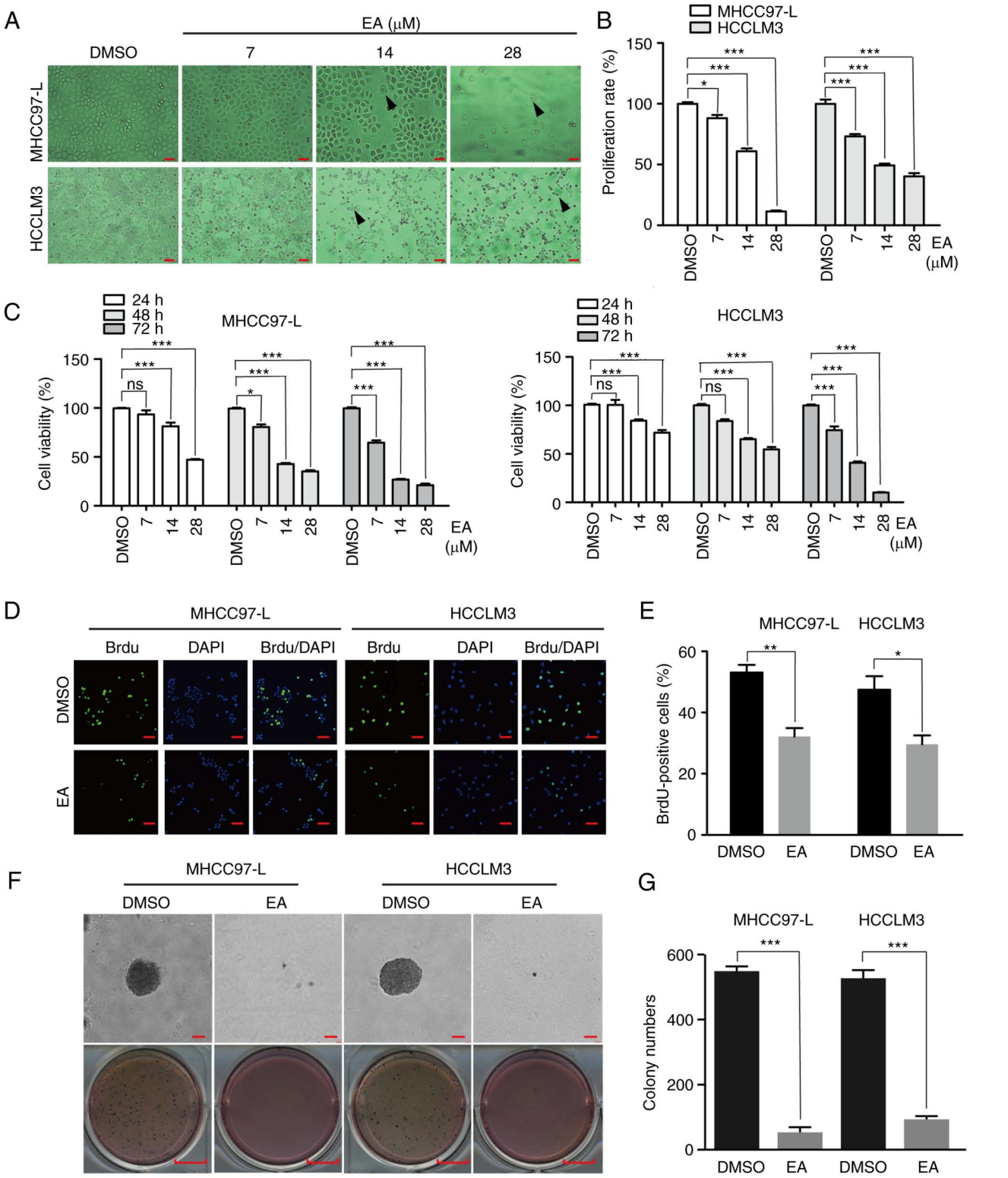

Figure 1. Effect of EA on the proliferation of human hepatocellular carcinoma cells *in vitro*. (A) Morphology of MHCC97-L and HCCLM3 cells after EA treatment for 48 h. Arrows indicate morphologically altered cells. Scale bar, 100 μm. (B) Proliferation rate of MHCC97-L and HCCLM3 cells after EA treatment for 48 h. Scale bar, 100 mm. Representative of biologically independent samples, n=5. (C) Viability of MHCC97-L and HCCLM3 cells after EA treatment for 1, 2 or 3 days. At each time point, DMSO was regarded as the control group. n=6. (D) Image of MHCC97-L and HCCLM3 cells positive for BrdU staining after EA treatment for 48 h. Scale bar, 100 μm. Representative of biologically independent samples, n=3. (E) Quantification of BrdU-positive MHCC97-L and HCCLM3 cells in (D). (F) Effects of EA on colony formation in MHCC97-L and HCCLM3 cells. (G) Colony numbers in (F) were quantified. Scale bar, 100 μm. n=3. All data are shown as the mean ± SD. *P<0.05, **P<0.01, ***P<0.001. EA, eupalinolide A; BrdU, 5-bromo-2-deoxyuridine.

reduced (Fig. 1D and E). The soft agar assay further revealed smaller and fewer colonies following EA treatment (28 μM EA for 48 h) compared with the colonies in the DMSO group (Fig. 1F and G). These results suggested that EA markedly inhibited the viability and proliferation of human hepatocellular carcinoma cells.

EA suppresses the migration of human hepatocellular carcinoma cells. Surgical resection remains the main treatment method for hepatocellular carcinoma and it significantly reduces the mortality of patients with hepatocellular carcinoma; however, the postoperative recurrence rate remains high at >70% (24). Therefore, the present study assessed whether EA affected cell motility using the wound-healing assay. Notably, there was a significant decrease in cell migration following EA treatment for 24 and 48 h compared with that in the DMSO group (Fig. 2A and B). The results of Transwell assays were similar to the results of the wound-healing assay (Fig. 2C and D). E-cadherin, Vimentin, N-cadherin, fibronectin and ZEB1 are major canonical markers of the epithelial-mesenchymal transition (EMT), which serve crucial roles in the tumor migration process (25). In the present study, E-cadherin, N-cadherin, fibronectin and ZEB1 were significantly upregulated, whereas Vimentin was significantly downregulated following EA treatment in a dose-dependent manner (Figs. 2E and F, and S1A and B). These results suggested that EA treatment reversed the EMT of human hepatocellular carcinoma cells, thus strongly inhibiting their migration.

EA induces cell cycle arrest at the G_1 phase. The proliferation of tumor cells is determined by cell cycle progression (26). Antitumor drugs can be divided into cell cycle-specific and non-specific drugs (27). In the present study, the effect of EA on the cell cycle was examined using flow cytometry. The percentage of MHCC97-L and HCCLM3 cells in the G_1 phase was significantly increased following treatment with 14 and 28 μM EA for 48 h compared with the control cells (Fig. 3A and B). Notably, the expression levels of CDK2, CDK4, cyclin E1 and cyclin D1, the key regulators for G_1 phase transition (28), were downregulated following treatment with 14 and 28 μM EA (Figs. 3C and D, and S1C and D). These results demonstrated that EA induced G_1-phase arrest by affecting the expression of cell cycle regulatory proteins.

EA does not affect apoptosis and necrosis. Apoptosis and necrosis are the major cell death mechanisms (29), and numerous antitumor drugs exert their effects by inducing apoptosis or necrosis (30,31). The present study therefore investigated whether EA treatment caused apoptosis and necrosis of hepatocellular carcinoma cells by detecting the expression levels of apoptosis- and necrosis-related proteins using western blot analysis following treatment of the cells with 7, 14 and 28 μM EA for 48 h. Notably, EA treatment did not affect the expression levels of cleaved-PARP and cleaved-caspase-3, which are apoptosis-related proteins, nor those of RIP1 and p-MLKL, which are necrosis-related proteins (Fig. 4A and B). The Annexin V-FITC/PI apoptosis assay conducted using flow cytometry further revealed that EA did not induce early or late apoptosis (Fig. 4C and D). Furthermore, treatment with the apoptosis inhibitor (Z-VAD-FMK) and necrosis inhibitor (necrostatin-1) did not restore the EA-induced decrease in cell viability (Fig. 4E). These results suggested that EA-induced inhibition of human hepatocellular carcinoma cell viability was independent of apoptotic and necroptotic factors.

EA induces autophagy and ROS activation in human hepatocellular carcinoma cells. Autophagy is a classic type of programmed cell death that participates in the functional modulation of cancer cells by affecting Atg proteins (32). The present study investigated whether EA served an anti-liver cancer role by inducing autophagy. Notably, EA upregulated the expression levels of LC3 II/I and Atg5, but downregulated p62/SQSTM1 expression, compared with those in the DMSO group (Fig. 5A-F). LC3 II/I, Atg5 and p62/SQSTM1 are autophagy biomarkers. Autophagosomes, which are two-layered structures containing cytoplasmic components, were formed following treatment with 28 μM EA (Fig. 5G). ROS regulate the autophagy pathway in cancer cells (33-35). Notably, excessively high levels of ROS can induce cell death through oxidative damage (36). In the present study, EA strongly induced ROS production compared with in DMSO cells (Fig. 5H and I). Treatment with the pharmacological inhibitor of autophagy 3-MA and anti-ROS reagent NAC efficiently reversed the EA-induced inhibition of cell viability and migration (Fig. 5J and K). These results suggested that autophagy and ROS activation potentially contributed to human hepatocellular carcinoma cell death and defects in migration induced by EA.

EA treatment activates the ERK/MAPK signaling pathway in human hepatocellular carcinoma cells. Abnormal activation of the MAPK signaling pathway is closely related to the occurrence, development and metastasis of hepatocellular carcinoma (37). In the present study, transcriptome analysis, which was conducted to investigate the mechanism underlying EA-induced cell death and migration, revealed that gene expression levels were significantly altered after EA treatment compared with in the control group (Fig. 6A). According to the KEGG pathway enrichment analysis results of differentially expressed genes, the top 10 pathways with the minimum P-value or the most significant enrichment were selected (Fig. 6B). The present study focused on the 'MAPK signaling pathway'. Further validation of the transcriptome sequencing data using western blotting revealed that EA significantly upregulated p-ERK expression, but did not affect p-p38 and p-JNK expression, in MHCC97-L and HCCLM3 cells compared with in the DMSO group (Figs. 6C and S2A). Furthermore, the decreased cell viability and migration induced by EA were reversed by ERK inactivation using PD98059 (Fig. 6E-G). These results suggested that ERK signaling participated in EA-induced cell death and migration inhibition.

EA induces autophagy via the ROS/ERK signaling pathway. A ROS scavenger (NAC) and ERK-specific inhibitor (PD98059) were used to investigate the interplay between ROS and ERK in EA-induced autophagy using western blotting. Pretreatment with NAC significantly reduced the activation of p-ERK and LC3 II/I induced by EA in both MHCC97-L and HCCLM3 cells, indicating that ROS was an upstream signal of EA and induced ERK activation and autophagy (Fig. 7A-D). Notably, the ERK-specific inhibitor PD98059 also suppressed the EA-induced increased expression of p-ERK and LC3 II/I in both MHCC97-L and HCCLM3 cells (Fig. 7E-H). These data suggested that EA induced autophagy by activating ROS production and ERK signaling.

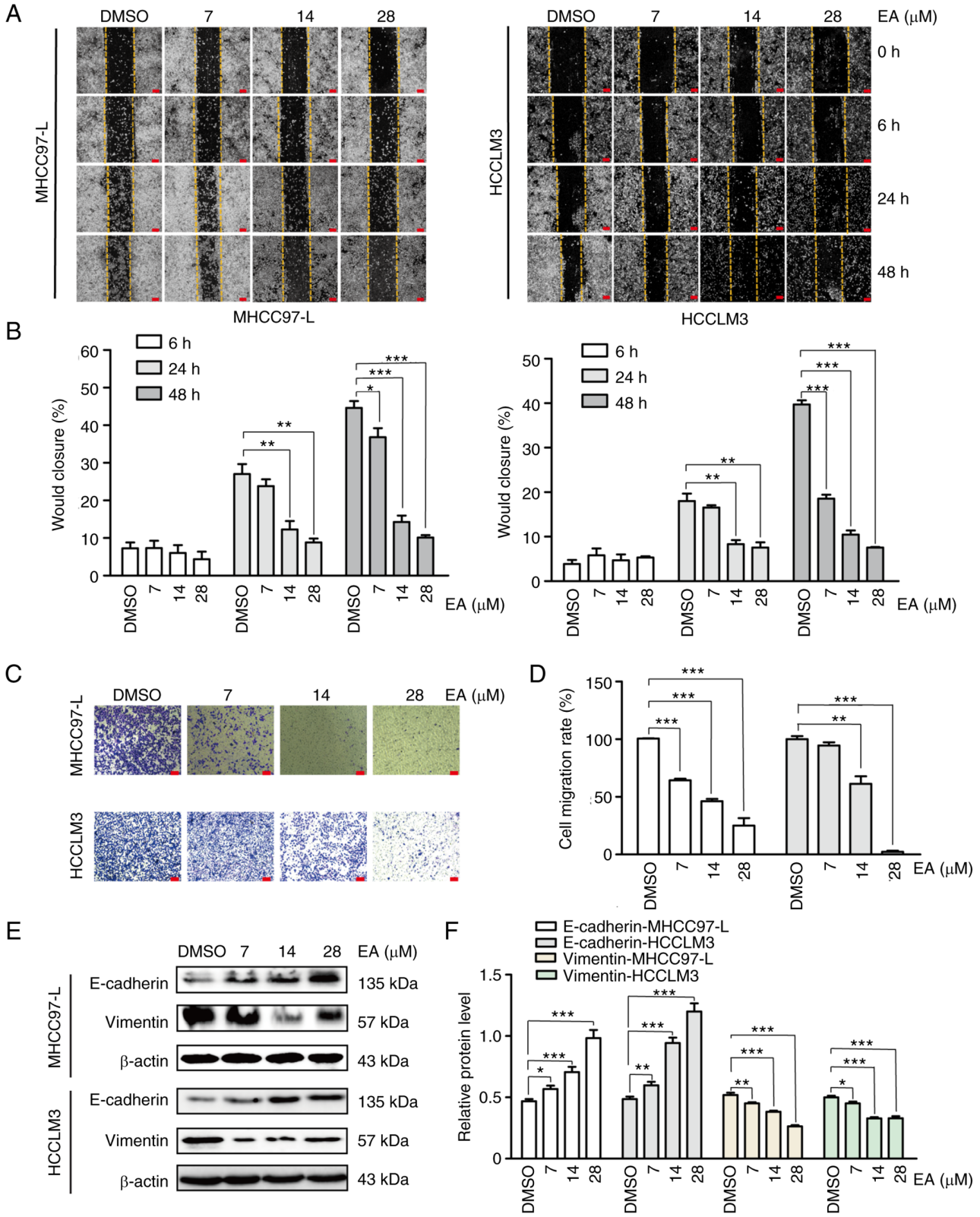

Figure 2. Effect of EA on the migration of human hepatocellular carcinoma cells. (A and B) Migration of MHCC97-L and HCCLM3 cells following treatment with EA for the indicated durations, as determined by wound-healing assay. Scale bar, 250 μm. Representative of biologically independent samples, n=3. (C and D) Migration of MHCC97-L and HCCLM3 cells following treatment with EA for 24 h, as determined by Transwell migration assay. Scale bar, 100 μm. Representative of biologically independent samples, n=5. (E and F) Western blot analysis of the expression levels of EMT-related proteins at 48 h in MHCC97-L and HCCLM3 cells. β-actin was used as a control. All data are shown as the mean ± SD. *P<0.05, **P<0.01, ***P<0.001. EA, eupalinolide A.

EA inhibits tumor growth in vivo. In vivo assays using nude mice were further performed to determine whether EA inhibited the growth of hepatocellular carcinoma. Nude mice were subcutaneously inoculated with 1x10^{6} hepatocellular carcinoma cells. The mice were subsequently intraperitoneally injected with EA or DMSO (control) daily for 21 days, followed

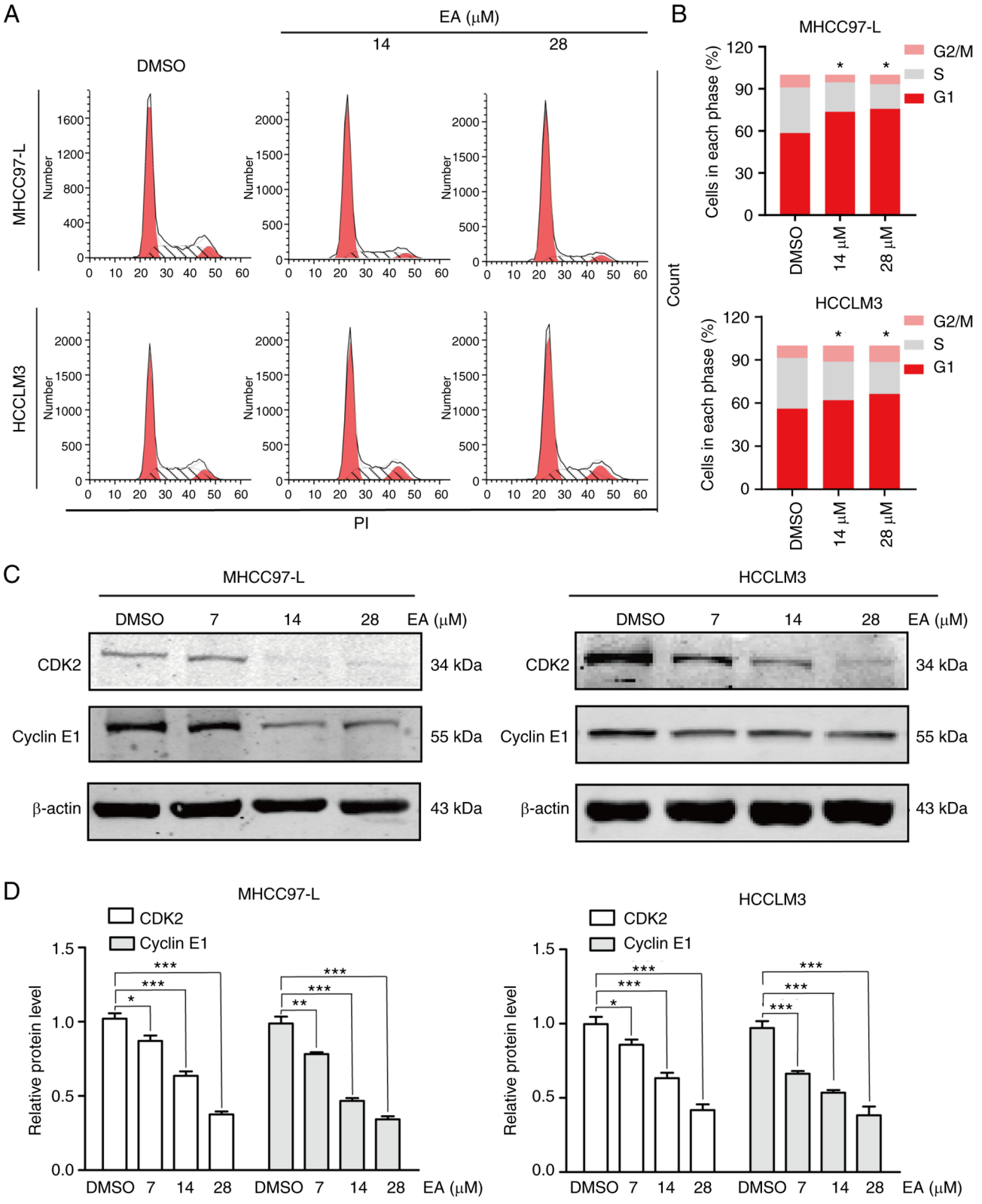

Figure 3. Effect of EA on the cell cycle progression of human hepatocellular carcinoma cells. (A) Cell cycle progression of MHCC97-L and HCCLM3 cells was analyzed by flow cytometry following EA treatment. (B) Percentage of MHCC97-L and HCCLM3 cells in each phase of the cell cycle. n=5. (C and D) Western blot analysis of the expression levels of cell cycle-related proteins at 48 h in MHCC97-L and HCCLM3 cells. β-actin was used as a control. All data are shown as the mean ± SD. *P<0.05, **P<0.01, ***P<0.001. EA, eupalinolide A.

by an assessment of tumor growth following cessation of treatment. Mice treated with EA exhibited a smaller tumor volume and weight than mice in the control group (Fig. 8A-C), thus indicating that EA markedly inhibited tumor growth *in vivo*.

Discussion

The present study investigated the effect of EA on hepatocellular carcinoma. *In vitro*, MHCC97-L and HCCLM3 cell lines

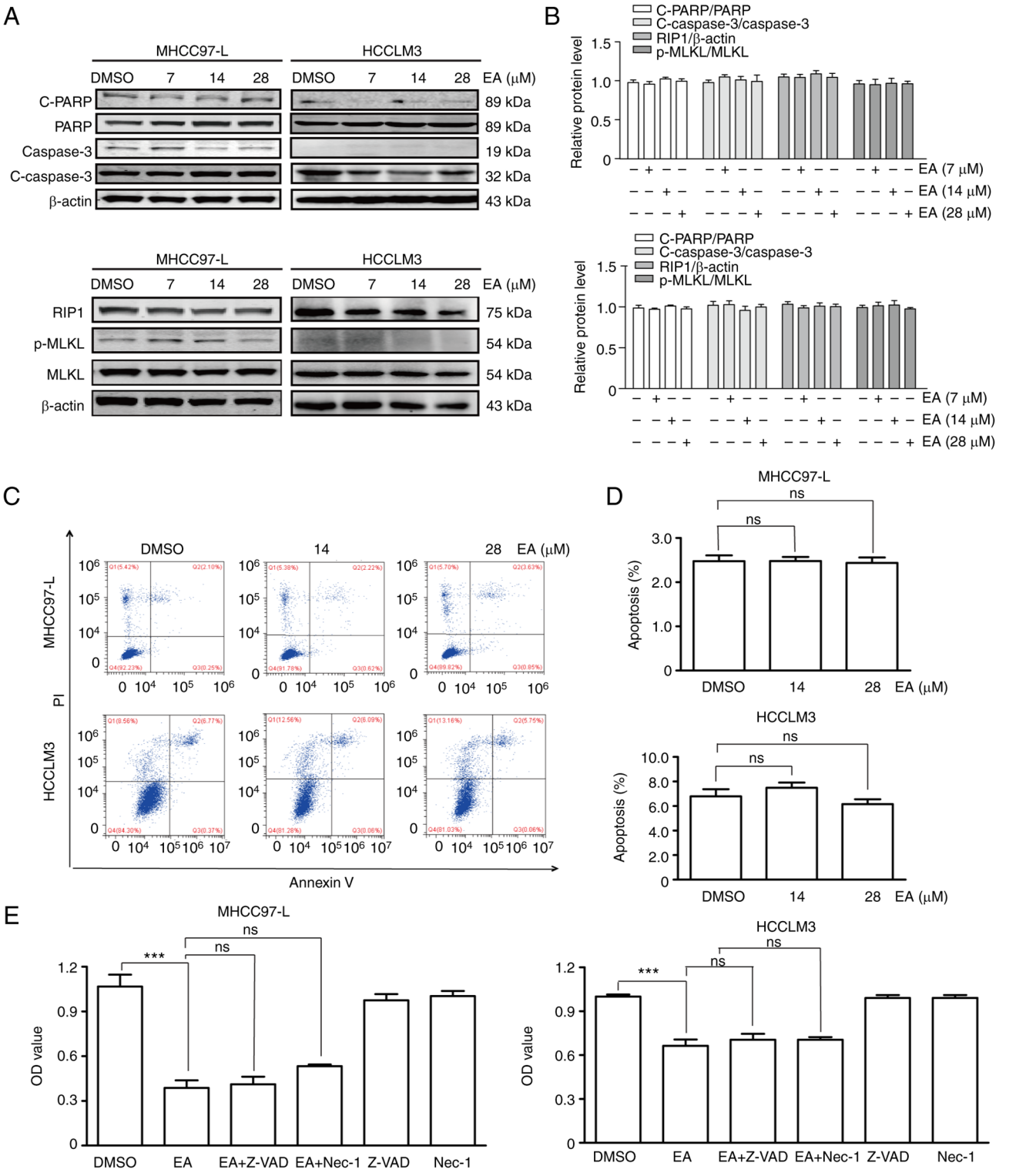

Figure 4. Effect of EA on apoptosis and necroptosis of human hepatocellular carcinoma cells. (A and B) Western blot analysis of the expression levels of apoptosis and necroptosis-related proteins at 48 h in MHCC97-L and HCCLM3 cells. β-actin was used as a control. (C and D) Effect of EA on apoptosis in MHCC97-L and HCCLM3 cells, as determined by flow cytometry. n=5. (E) Viability of MHCC97-L and HCCLM3 cells treated with or without apoptosis or necroptosis inhibitors was measured by Cell Counting Kit 8 assays. n=6. All data are shown as the mean ± SD. ***P<0.001. EA, eupalinolide A; C-, cleaved; p-, phosphorylated.

were selected because MHCC97-L is a human hepatocellular carcinoma cell line with low metastatic potential and HCCLM3 is a human hepatocellular carcinoma cell line with high metastatic potential. In addition, MHCC97-L and HCCLM3 cell lines have been adopted in a number of studies (38,39).

The present study revealed that EA inhibited the growth of hepatocellular carcinoma cells *in vivo* and *in vitro*. The *in vitro* results demonstrated that EA caused cell cycle arrest at the G_1 phase and induced cell autophagy via the ROS/ERK signaling pathway. By contrast, treatment with a ROS scavenger, ERK

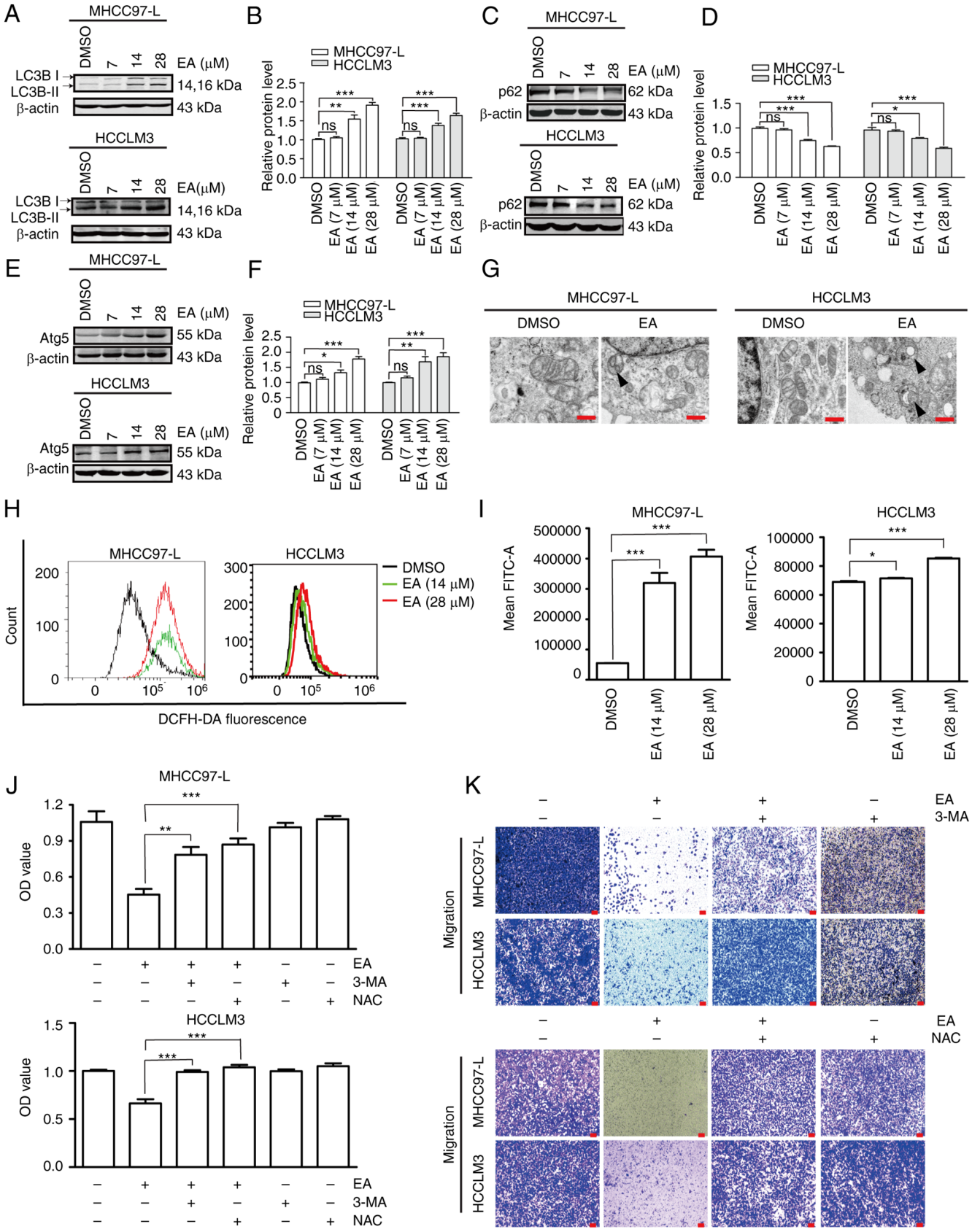

Figure 5. Effect of EA on the autophagy of human hepatocellular carcinoma cells. (A-F) Western blot analysis of the expression levels of autophagy-related proteins at 48 h in MHCC97-L and HCCLM3 cells. β-actin was used as a control. (G) Transmission electron microscopy of MHCC97-L and HCCLM3 cells following EA treatment for 48 h. Arrow indicates autophagosomes. Scale bar, 500 nm. (H and I) ROS production of MHCC97-L and HCCLM3 cells was measured by DFC fluorescence following EA treatment. Representative of biologically independent samples, n=6. (J) Viability of MHCC97-L and HCCLM3 cells treated with or without ROS or autophagy inhibitors, as measured by Cell Counting Kit 8 assays. Representative of biologically independent samples, n=6. (K) Migratory ability of MHCC97-L and HCCLM3 cells treated with or without ROS or autophagy inhibitors, as measured by Transwell migration assays after EA treatment. All data are shown as the mean ± SD. *P<0.05, **P<0.01, ***P<0.001. EA, eupalinolide A; Atg5, autophagy-related 5; 3-MA, 3-methyladenine; NAC, N-acetylcysteine; ROS, reactive oxygen species.

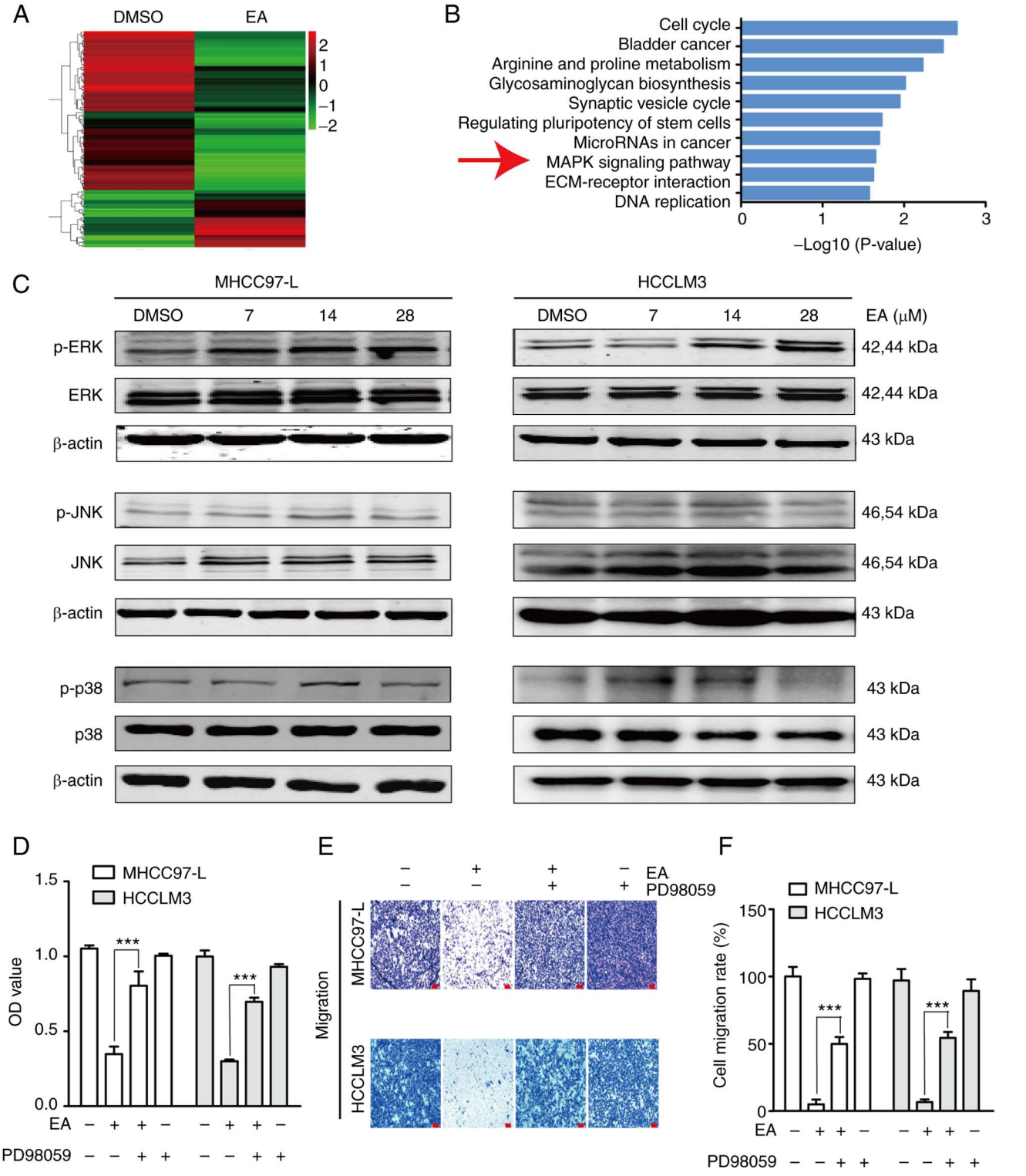

Figure 6. Effect of EA on MAPK signaling in human hepatocellular carcinoma cells. (A) Heatmap showing differential gene expression in HCCLM3 cells with or without 28 μM EA treatment for 48 h. (B) KEGG analysis of genes in HCCLM3 cells. The top 10 KEGG pathways based on fold enrichment are shown. The arrow indicates the 'MAPK signaling pathway'. (C) Western blot analysis of the expression levels of MAPK-related protein at 48 h in MHCC97-L and HCCLM3 cells. β-actin was used as a control. (D) Viability of MHCC97-L and HCCLM3 cells treated with or without an ERK inhibitor was measured by Cell Counting Kit 8 assay. n=6. (E and F) Migratory ability of MHCC97-L and HCCLM3 cells treated with or without an ERK inhibitor, as measured by Transwell migration assays after EA treatment. All data are shown as the mean ± SD. ***P<0.001. EA, eupalinolide A; p-, phosphorylated; KEGG, Kyoto Encyclopedia of Genes and Genomes.

inhibitor or autophagy inhibitor reversed the decrease in cell viability and migration induced by EA. The ROS scavenger induced a nearly complete recovery of the proliferative and migratory ability of hepatocellular carcinoma cells. The anti-hepatocellular carcinoma mechanism of EA is summarized in Fig. 9.

Several types of traditional Chinese medicine have been explored for their use in the treatment of cancer (40,41). Our

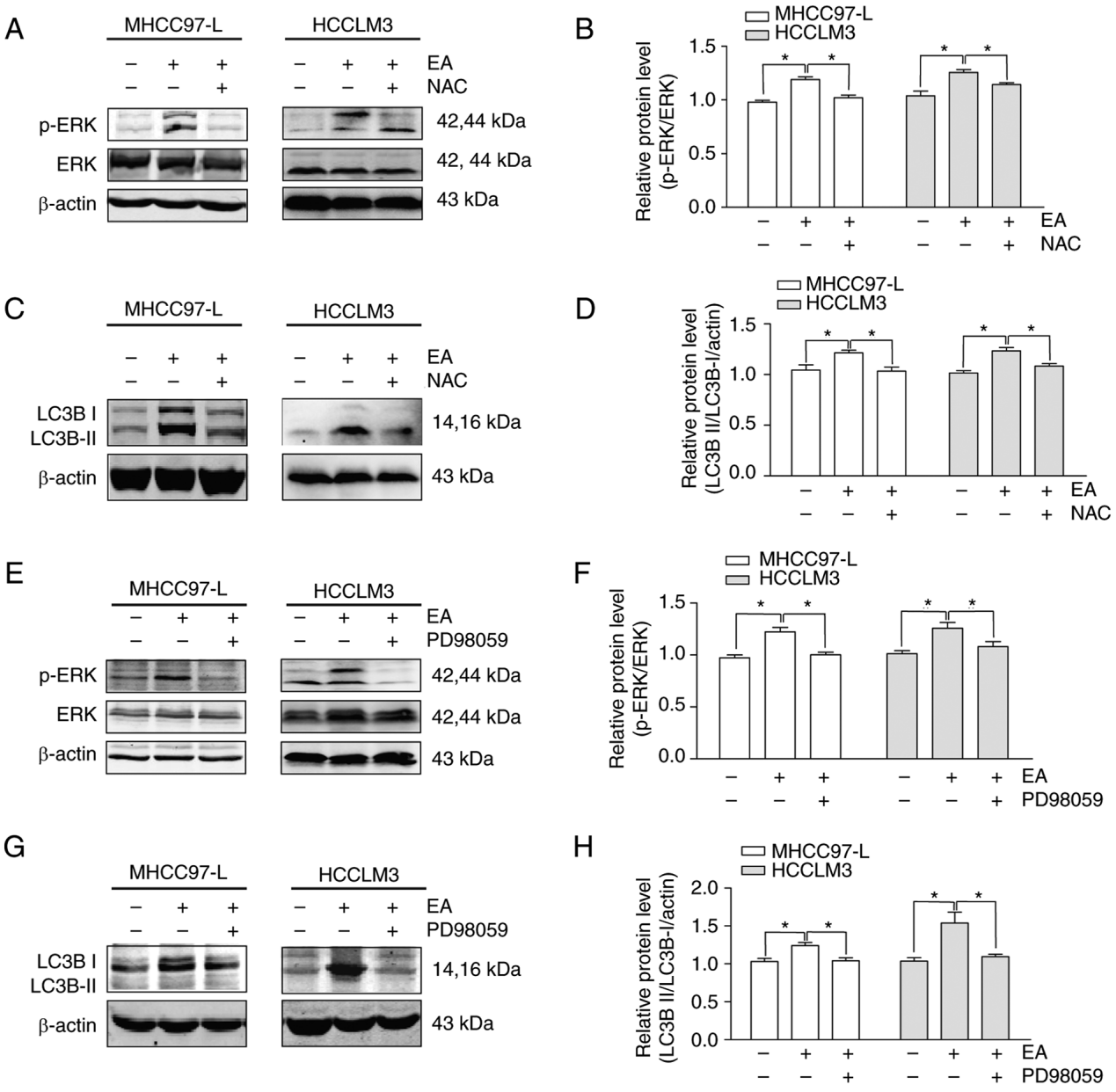

Figure 7. Effect of EA on the ROS/ERK signaling pathway in human hepatocellular carcinoma cells. (A-D) Western blot analysis of the protein expression levels of p-ERK and LC3 II/I at 48 h in MHCC97-L and HCCLM3 cells treated with or without a ROS inhibitor. β-actin was used as a control. (E-H) Western blot analysis of the protein expression levels of p-ERK and LC3 II/I at 48 h in MHCC97-L and HCCLM3 cells treated with or without the ERK inhibitor PD98059. β-actin was used as a control. All data are shown as the mean ± SD. *P<0.05. EA, eupalinolide A; NAC, N-acetylcysteine; p-, phosphorylated.

research team has aimed to identify a new drug for treating liver cancer. EL has been widely applied to treat respiratory diseases, because of its antihypertensive, antiviral and anti-tumor effects. In the present study, EA markedly reduced the proliferation of MHCC97-L and HCCLM3 cells. EA, especially at 28 μM, led to a number of floating cells, a change in cell morphology and death of most MHCC97-L and HCCLM3 cells. These results demonstrated that EA had a powerful hepatocellular carcinoma cell-killing ability *in vitro*.

Chemotactic migration is vital for the invasion of cancer cells into the surrounding tissue, resulting in tumor metastasis (42). In the present study, the migratory ability of hepatocellular carcinoma cells was inhibited by EA, especially at 28 μM. Notably, the invasive and metastatic ability of carcinoma cells has been reported to be promoted by EMT (43). E-cadherin has a vital role in maintaining the integrity of intercellular junctions in cell adhesion. Loss of E-cadherin expression can lead to a loss of contact, increased cell motility and cancer advancement (44). Vimentin has been shown to be overexpressed in gastrointestinal tumors, and usually aggravates tumor growth and invasion, leading to poor prognosis (45). In the present study, EA inhibited EMT by increasing the expression levels of E-cadherin and decreasing those of Vimentin. In addition, EA can affect the expression of other EMT-related proteins, including N-cadherin, fibronectin and ZEB1. EA thus inhibited the migration of hepatocellular carcinoma cells by reversing EMT progression.

Most human somatic cells experience a fixed life cycle through a highly coordinated and regulated process; however, faults occur during the cell cycle in cancer cells, resulting in

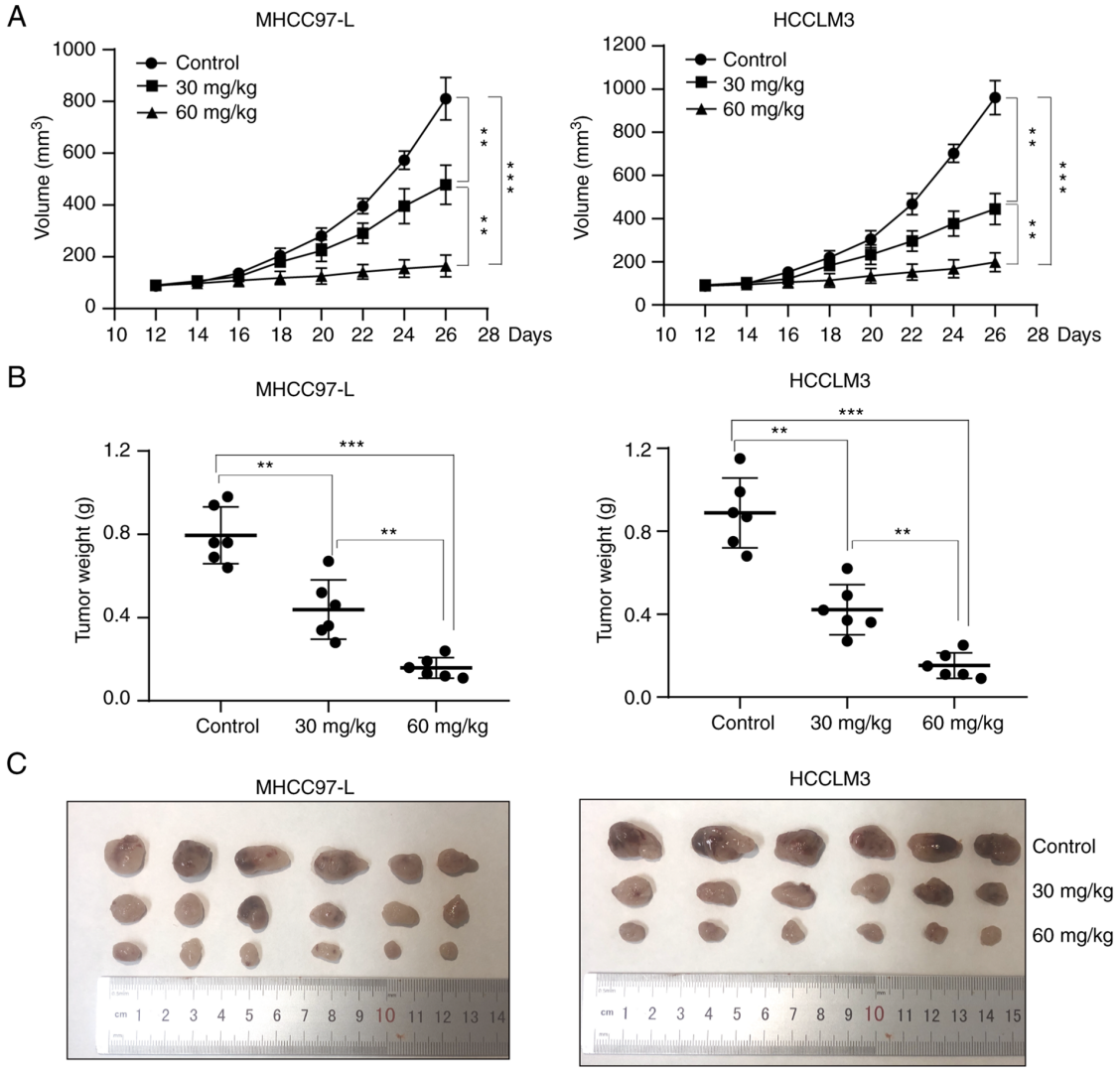

Figure 8. Effect of EA on tumor growth in a xenograft model of human hepatocellular carcinoma cells *in vivo*. (A) MHCC97-L and HCCLM3 xenograft tumor volume. n=6. (B) Weight of xenograft tumors formed by MHCC97-L and HCCLM3 cells. n=6. (C) Images of MHCC97-L and HCCLM3 cell xenograft tumors treated with or without EA treatment. All data are shown as the mean ± SD. **P<0.01, ***P<0.001. EA, eupalinolide A.

unchecked cell growth (46). Numerous anticancer drugs, such as vincristine and colchicine, induce cell cycle arrest (47,48). In the present study, EA arrested the cell cycle at the G_1 phase, which is similar to the effect of vinblastine, by regulating the cell cycle phase checkpoint proteins such as Cyclin E and CDK2 (49). These results indicated that EA exerted an anticancer effect by arresting the cell cycle.

Apoptosis and necrosis are classic cell death mechanisms and promising targets in anticancer therapy (40,50,51). In the present study, EA had no significant effect on apoptosis and necrosis. Moreover, apoptosis and necrosis inhibitors did not reverse the EA-induced decrease in cell viability. These results suggested that EA induced cell death independent of apoptosis and necrosis.

Autophagy and ROS are involved in cell survival and cell death pathways. A number of anticancer drugs activate autophagy and ROS signaling (52,53). Autophagy is a dynamic process of protein degradation that usually occurs during nutrient deprivation. Autophagy serves dual roles in cancer by acting as a tumor suppressor and a tumor promoter that accelerates the growth of established tumors (54). Autophagy is thus a common target for drugs used to treat cancer. The LC3 II/I ratio is used to estimate the level of autophagy. p62/SQSTM1 binds directly to Atg8/LC3 to facilitate the degradation of ubiquitinated proteins aggregated by autophagy. The overexpression of Atg5 can also enhance autophagy (55,56). In the present study, EA significantly activated the autophagy signal biomarker LC3 II/I and Atg5, and suppressed the expression of p62. Furthermore, EA induced autophagy in hepatocellular carcinoma cells, which was verified by electron microscopic observation. Autophagy is categorized into macro-autophagy, micro-autophagy and chaperone-mediated autophagy (57). EA-induced autophagy belongs to macro-autophagy, which is characterized by the formation of autophagosomes and autolysosomes. ROS is an important upstream molecule that regulates cancer cell death and survival; excessive levels of ROS can cause oxidative damage to cancer cells (58). In the present study, EA significantly increased ROS generation in hepatocellular carcinoma cells; however, treatment with the ROS scavenger NAC and autophagy-specific inhibitor 3-MA reversed EA-induced inhibition of cell proliferation and migration. These results indicated that ROS and autophagy were involved in EA-induced cell death.

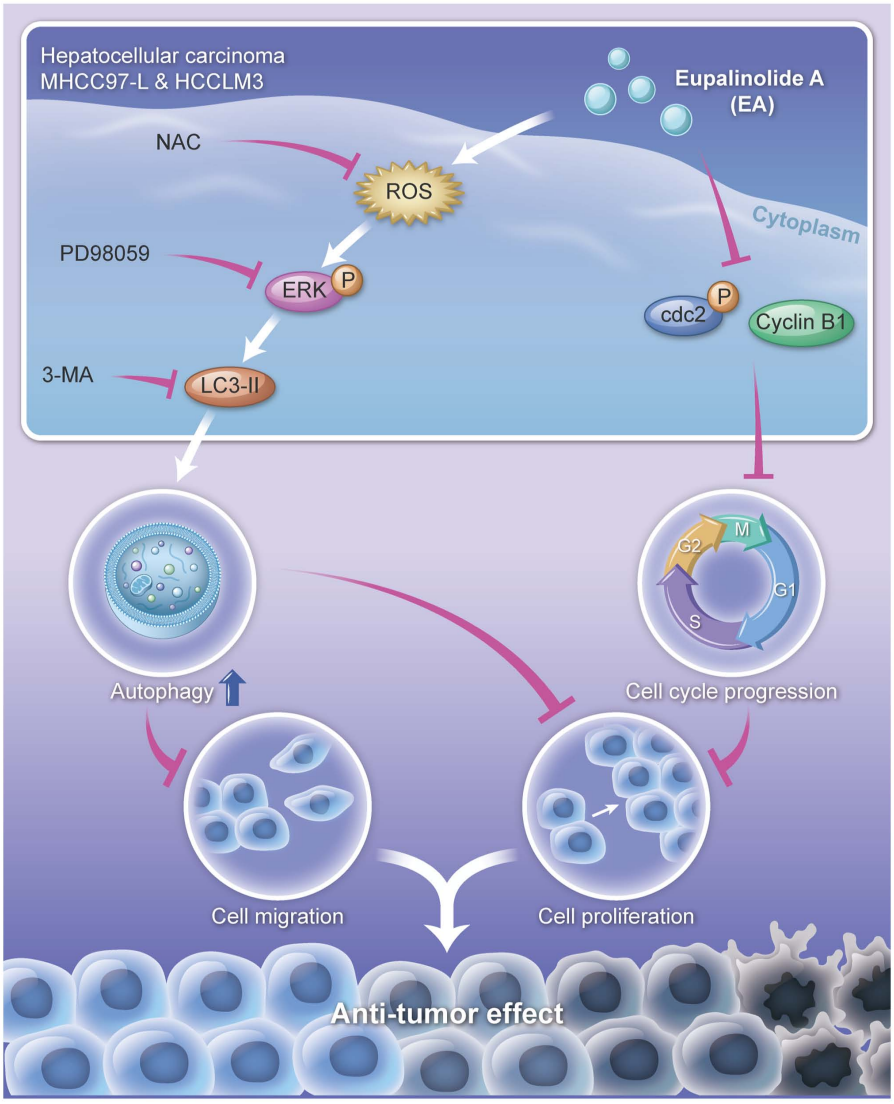

Figure 9. Diagram showing the mechanism in which EA inhibits hepatocellular carcinoma by inducing autophagy and blocking the cell cycle. NAC, N-acetylcysteine; 3-MA, 3-methyladenine; ROS, reactive oxygen species.

A number of signals are involved in regulating ROS and autophagy in cancer. The MAPK signaling pathway, a downstream pathway of ROS, is known to have an essential role in inducing autophagy (59,60). In the present study, there was an increase in the phosphorylation of ERK. The specific inhibitor PD98059 also partially reversed EA-induced inhibition of cell viability and migration. Furthermore, the ROS scavenger NAC almost abolished the effect of EA on p-ERK and LC3 II/I. The *in vivo* study also indicated that EA inhibited the growth of hepatocellular carcinoma xenografts.

EL mainly contains flavonoids, sesquiterpenoids, diterpenoids, triterpenoids, volatile oils, organic acids, amino acids, trace elements and other bioactive substances, and has been used for the clinical treatment of tracheitis. In recent years, numerous scientists have focused on studying the role of EL in cancer. EL extracts, including eupalinolide O, eupalinolide J and other sesquiterpene lactones, have been reported to serve vital roles in breast and prostate cancer (10,23,61). In the present study, EA inhibited liver cancer *in vitro* and *in vivo*. These findings indicated that EL and other similar sesquiterpene lactones may be potential anticancer drugs. However, the mechanisms of other sesquiterpene lactones in cancer should be investigated further. EA is a promising candidate for treating hepatocellular carcinoma, as the present study indicated that it may induce cell autophagy via the ROS/ERK signaling pathway *in vitro* and *in vivo*.

Acknowledgements

The authors thank Sagene eBioart for their help in generating Fig. 9.

Funding

This work was supported by the Science and Technology Research Program of Chongqing Municipal Education Commission (grant nos. KJZD-K201902701 and KJQN201802702), the Chongqing Natural Science Foundation of Chongqing Science and Technology Bureau (grant no. cstc2019jcyj-msxmX0607), the Natural Science Research Program of Chongqing Three Gorges Medical College (grant nos. 2018xzz01 and 2019XZZ004), the Chongqing Key

Disciplines of Traditional Chinese Medicine (Basic Theory of Traditional Chinese Medicine) Construction Project (grant no. 16, 2021), the Young and middle-aged Top-notch Talent Support Program of Chongqing Three Gorges Medical College, Bayu scholar program, and Chongqing University Innovation Group Project (grant no. CXQT20030).

Availability of data and materials

The RNA sequencing datasets used and/or analyzed during the current study are available from https://www.ncbi.nlm.nih.gov/sra/?term=PRJNA805012. The non-sequencing data are available from the corresponding author on reasonable request.

Authors' contributions

GL, CZ and YZ conceived and designed the study. FD, ZC, TW, LP, WL, LJ, HL and JL performed the experiments. WD, HZ, JM, MH, YW, XD, DL and PH acquired, analyzed and interpretated the data. GZ and YP conducted statistical analysis. GL, CZ and YZ confirmed the authenticity of all the raw data. All authors read and approved the final version of the manuscript.

Ethics approval and consent to participate

The animal experiments were reviewed and approved (approval no. 2022-SCSL-KY-001) by the medical ethics committee of the Affiliated Hospital of Chongqing Three Gorges Medical College (Chongqing, China).

Patient consent for publication

Not applicable.

Competing interests

The authors declare that they have no competing interests.

References

1. Zheng RS, Zhang SW, Zeng HM, Wang SM, Sun KX, Chen R, Li L, Wei WQ and He J: Cancer incidence and mortality in China, 2016. J Nat Cancer Cent 2: 1-9, 2022.
2. Forner A, Reig M and Bruix J: Hepatocellular carcinoma. Lancet 391: 1301-1314, 2018.
3. Liu CY, Chen KF and Chen PJ: Treatment of liver cancer. Cold Spring Harb Perspect Med 5: a021535, 2015.
4. Chen S, Cao Q, Wen W and Wang H: Targeted therapy for hepatocellular carcinoma: Challenges and opportunities. Cancer Lett 460: 1-9, 2019.
5. Llovet JM, Montal R, Sia D and Finn RS: Molecular therapies and precision medicine for hepatocellular carcinoma. Nat Rev Clin Oncol 15: 599-616, 2018.
6. Li Y, Gao ZH and Qu XJ: The adverse effects of sorafenib in patients with advanced cancers. Basic Clin Pharmacol Toxicol 116: 216-221, 2015.
7. Heo YA and Syed YY: Regorafenib: A review in hepatocellular carcinoma. Drugs 78: 951-958, 2018.
8. Wang X, Ma S, Lai F, Wang Y and Lou C: Traditional applications, phytochemistry, and pharmacological activities of *Eupatorium lindleyanum* DC.: A comprehensive review. Front Pharmacol 8: 577124, 2020.
9. Chi D: Study on the antihypertensive effects of water decoction of *Eupatorium lindleyanum* on spontaneously hypertensive rats and corresponding mechanism. China Pharm 27: 3502-3504, 2016.
10. Lou C, Chen Y, Zhang J, Yang B and Zhao H: Eupalinolide J suppresses the growth of triple-negative breast cancer cells via targeting STAT3 signaling pathway. Front Pharmacol 10: 1071, 2019.
11. Peng Y, Dou J, Huang F and Qian D: Antiviral effects of Fufang Yemazhui capsule in vitro and in vivo. Chin Tradit Pat Med 30: 650-654, 2008.
12. Chen WY, Qin J, He HX, Li Q, Wang KJ and Zhou YD: Effects of lindley eupatorium herb total flavonoid on blood lipid metabolism in experimental hyperlipidemic rats. J Third Mil Med Univ 31: 1589-1591, 2009.
13. Cu CJ, Ren HL and Wu TW: Study on the chemical constituents and antipyretic action of *Eupatorium lindleyanum* DC. Nat Prod Res Dev 5: 816-821, 2015.
14. Wang J, Wu M, Zheng D, Zhang H, Lv Y, Zhang L, Tan HS, Zhou H, Lao YZ and Xu HX: Garcinol inhibits esophageal cancer metastasis by suppressing the p300 and TGF-β1 signaling pathways. Acta Pharmacol Sin 41: 82-92, 2020.
15. Zhang YH, Pan LH, Pang Y, Yang JX, Lv MJ, Liu F, Qu XF, Chen XX, Gong HJ, Liu D and Wei Y: GDF11/BMP11 as a novel tumor marker for liver cancer. Exp Ther Med 15: 3495-3500, 2018.
16. Yue SR, Tan YY, Zhang L, Zhang BJ, Jiang FY, Ji G, Liu BC and Wang RR: Gynostemma pentaphyllum polysaccharides ameliorate non-alcoholic steatohepatitis in mice associated with gut microbiota and the TLR2/NLRP3 pathway. Front Endocrinol (Lausanne) 13: 885039, 2022.
17. Anders S and Huber W: Differential expression analysis for sequence count data. Genome Biol 11: R106, 2010.
18. Yu G, Wang LG, Han Y and He QY: clusterProfiler: An R package for comparing biological themes among gene clusters. OMICS 16: 284-287, 2012.
19. Zhang Y, Li M, Li L, Qian G, Wang Y, Chen Z, Liu J, Fang C, Huang F, Guo D, *et al*: β-arrestin 2 as an activator of cGAS-STING signaling and target of viral immune evasion. Nat Commun 11: 6000, 2020.
20. Wang Y, Qian G, Zhu L, Zhao Z, Liu Y, Han W, Zhang X, Zhang Y, Xiong T, Zeng H, *et al*: HIV-1 Vif suppresses antiviral immunity by targeting STING. Cell Mol Immunol 19: 108-121, 2022.
21. Piñero F, Dirchwolf M and Pessôa MG: Biomarkers in hepatocellular carcinoma: Diagnosis, prognosis and treatment response assessment. Cells 9: 1370, 2020.
22. Yang B, Zhao Y, Lou C and Zhao H: Eupalinolide O, a novel sesquiterpene lactone from *Eupatorium lindleyanum* DC., induces cell cycle arrest and apoptosis in human MDA-MB-468 breast cancer cells. Oncol Rep 36: 2807-2813, 2016.
23. Yang B, Shen JW, Zhou DH, Zhao YP, Wang WQ, Zhu Y and Zhao HJ: Precise discovery of a STAT3 inhibitor from *Eupatorium lindleyanum* and evaluation of its activity of anti-triple-negative breast cancer. Nat Prod Res 33: 477-485, 2019.
24. Bekki Y, Von Ahrens D, Takahashi H, Schwartz M and Gunasekaran G: Recurrent intrahepatic cholangiocarcinoma-review. Front Oncol 11: 776863, 2021.
25. Nijkamp MM, Span PN, Hoogsteen IJ, van der Kogel AJ, Kaanders JH and Bussink J: Expression of E-cadherin and vimentin correlates with metastasis formation in head and neck squamous cell carcinoma patients. Radiother Oncol 99: 344-348, 2011.
26. Alenzi FQ: Links between apoptosis, proliferation and the cell cycle. Br J Biomed Sci 61: 99-102, 2004.
27. Johansson M and Persson JL: Cancer therapy: Targeting cell cycle regulators. Anticancer Agents Med Chem 8: 723-731, 2008.
28. Honda R, Lowe ED, Dubinina E, Skamnaki V, Cook A, Brown NR and Johnson LN: The structure of cyclin E1/CDK2: Implications for CDK2 activation and CDK2-independent roles. EMBO J 24: 452-463, 2005.
29. Su Z, Yang Z, Xu Y, Chen Y and Yu Q: Apoptosis, autophagy, necroptosis, and cancer metastasis. Mol Cancer 14: 48, 2015.
30. Denicourt C and Dowdy SF: Medicine. Targeting apoptotic pathways in cancer cells. Science 305: 1411-1413, 2004.
31. Amaravadi RK and Thompson CB: The roles of therapy-induced autophagy and necrosis in cancer treatment. Clin Cancer Res 13: 7271-7279, 2007.
32. Li X, He S and Ma B: Autophagy and autophagy-related proteins in cancer. Mol Cancer 19: 12, 2020.
33. Poillet-Perez L, Despouy G, Delage-Mourroux R and Boyer-Guittaut M: Interplay between ROS and autophagy in cancer cells, from tumor initiation to cancer therapy. Redox Biol 4: 184-192, 2015.

34. Park HS, Han JH, Park JW, Lee DH, Jang KW, Lee M, Heo KS and Myung CS: Sodium propionate exerts anticancer effect in mice bearing breast cancer cell xenograft by regulating JAK2/STAT3/ROS/p38 MAPK signaling. Acta Pharmacol Sin 42: 1311-1323, 2021.
35. He C, Lu S, Wang XZ, Wang CC, Wang L, Liang SP, Luo TF, Wang ZC, Piao MH, Chi GF and Ge PF: FOXO3a protects glioma cells against temozolomide-induced DNA double strand breaks via promotion of BNIP3-mediated mitophagy. Acta Pharmacol Sin 42: 1324-1337, 2021.
36. Schieber M and Chandel NS: ROS function in redox signaling and oxidative stress. Curr Biol 24: E453-R462, 2014.
37. Delire B and Stärkel P: The Ras/MAPK pathway and hepatocarcinoma: Pathogenesis and therapeutic implications. Eur J Clin Invest 45: 609-623, 2015.
38. Zhou SL, Zhou ZJ, Hu ZQ, Huang XW, Wang Z, Chen EB, Fan J, Cao Y, Dai Z and Zhou J: Tumor-associated neutrophils recruit macrophages and T-regulatory cells to promote progression of hepatocellular carcinoma and resistance to sorafenib. Gastroenterology 150: 1646-1658.e17, 2016.
39. Wu F, Yang LY, Li YF, Ou DP, Chen DP and Fan C: Novel role for epidermal growth factor-like domain 7 in metastasis of human hepatocellular carcinoma. Hepatology 50: 1839-1850, 2009.
40. Zhang YS, Shen Q and Li J: Traditional Chinese medicine targeting apoptotic mechanisms for esophageal cancer therapy. Acta Pharmacol Sin 37: 295-302, 2016.
41. Liu Y, Yang S, Wang K, Lu J, Bao X, Wang R, Qiu Y, Wang T and Yu H: Cellular senescence and cancer: Focusing on traditional Chinese medicine and natural products. Cell Prolif 53: e12894, 2020.
42. Yamaguchi H, Wyckoff J and Condeelis J: Cell migration in tumors. Curr Opin Cell Biol 17: 559-564, 2005.
43. Chaffer CL, San Juan BP, Lim E and Weinberg RA: EMT, cell plasticity and metastasis. Cancer Metastasis Rev 35: 645-654, 2016.
44. Mendonsa AM, Na TY and Gumbiner BM: E-cadherin in contact inhibition and cancer. Oncogene 37: 4769-4780, 2018.
45. Satelli A and Li S: Vimentin in cancer and its potential as a molecular target for cancer therapy. Cell Mol Life Sci 68: 3033-3046, 2011.
46. Suski JM, Braun M, Strmiska V and Sicinski P: Targeting cell-cycle machinery in cancer. Cancer Cell 39: 759-778, 2021.
47. Camplejohn RS: A critical review of the use of vincristine (VCR) as a tumour cell synchronizing agent in cancer therapy. Cell Tissue Kinet 13: 327-335, 1980.
48. Kumar A, Sharma PR and Mondhe DM: Potential anticancer role of colchicine-based derivatives: An overview. Anticancer Drugs 28: 250-262, 2017.
49. Chen TK, Tang MS, Jiang CX and Zeng BX: Effect of vincristine on proliferation and apoptosis of human gastric cancer BGC cells and its mechanism. Chin Tradit Herb Drugs 46: 7, 2015.
50. Pfeffer CM ang Singh ATK: Apoptosis: A target for anticancer therapy. Int J Mol Sci 19: 448, 2018.
51. Karsch-Bluman A, Feiglin A, Arbib E, Stern T, Shoval H, Schwob O, Berger M and Benny O: Tissue necrosis and its role in cancer progression. Oncogene 38: 1920-1935, 2019.
52. Azad MB, Chen Y and Gibson SB: Regulation of autophagy by reactive oxygen species (ROS): Implications for cancer progression and treatment. Antioxid Redox Signal 11: 777-790, 2009.
53. Gibson SB: A matter of balance between life and death: Targeting reactive oxygen species (ROS)-induced autophagy for cancer therapy. Autophagy 6: 835-837, 2010.
54. Yang ZJ, Chee CE, Huang S and Sinicrope FA: The role of autophagy in cancer: Therapeutic implications. Mol Cancer Ther 10: 1533-1541, 2011.
55. Pankiv S, Clausen TH, Lamark T, Brech A, Bruun JA, Outzen H, Øvervatn A, Bjørkøy G and Johansen T: p62/SQSTM1 binds directly to Atg8/LC3 to facilitate degradation of ubiquitinated protein aggregates by autophagy. J Biol Chem 282: 24131-2445, 2007.
56. Pyo JO, Yoo SM, Ahn HH, Nah J, Hong SH, Kam TI, Jung S and Jung YK: Overexpression of Atg5 in mice activates autophagy and extends lifespan. Nat Commun 4: 2300, 2013.
57. Mizushima N, Levine B, Cuervo AM and Klionsky DJ: Autophagy fights disease through cellular self-digestion. Nature 451: 1069-1075, 2008.
58. Moloney JN and Cotter TG: ROS signalling in the biology of cancer. Semin Cell Dev Biol 80: 50-64, 2018.
59. Liu Y and Fan D: Ginsenoside Rg5 induces G2/M phase arrest, apoptosis and autophagy via regulating ROS-mediated MAPK pathways against human gastric cancer. Biochem Pharmacol 168: 285-304, 2019.
60. Fan J, Ren D, Wang J, Liu X, Zhang H, Wu M and Yang G: Bruceine D induces lung cancer cell apoptosis and autophagy via the ROS/MAPK signaling pathway in vitro and in vivo. Cell Death Dis 11: 126, 2020.
61. Wu Z, Xu X, Dai L, Wang Y, Yang B, Zhao H and Lou C: Eupalinolide J induces apoptosis, cell cycle arrest, mitochondrial membrane potential disruption and DNA damage in human prostate cancer cells. J Toxicol Sci 45: 15-23, 2020.

This work is licensed under a Creative Commons Attribution-NonCommercial-NoDerivatives 4.0 International (CC BY-NC-ND 4.0) License.